KFUPM
Journal of Undergraduate Research International

Diamond Open Access 106

Article Material Science and Engineering

Optimizing Hydrogen Evolution Reaction Performance of $MoSe_2$ through Strategic Transition-Metal Doping: A Density Functional Theory Analysis

Zahra Ali Aljishi and Md Delowar Hossain*

Cite https://doi.org/10.64589/juri/231555

Submitted: May 05, 2026 **Revised:** May 16, 2026 **Accepted:** May 16, 2026

ABSTRACT

Two-dimensional transition-metal dichalcogenides (TMDs) have emerged as promising candidates for hydrogen evolution reaction (HER) because of their high specific surface areas and mechanical flexibilities. However, the catalytic activities of pristine TMDs are limited by the chemical inertness of their basal planes. In this study, spin-polarized density functional theory calculations are performed to investigate the effects of 3d- and 4d-transition-metal doping on the HER performance of the $MoSe_2$ basal plane. Transition-metal doping in $MoSe_2$ confirms the thermodynamic stability of the resulting systems; specifically, doping with early transition metals offers the highest lattice stability, whereas doping with late transition metals induces greater electronic perturbations. The adsorption energetics reveal that pristine $MoSe_2$ provides the weakest binding energy toward H ($\Delta G_{H^*} = 1.40$ eV), whereas Zn doping gives the strongest binding energy ($\Delta G_{H^*} = -0.40$ eV). Moreover, doping of Cd and Ag in the nearest-neighbor configuration drastically reduces the Gibbs free energy of H adsorption to near-optimal values of –0.02 and –0.16 eV, respectively. Finally, electronic structure analysis and d-band center scaling indicate that these dopants trigger a semiconductor-to-metal transition and optimize the orbital hybridization between the metal d-states and H s-orbitals. These findings provide a theoretical foundation for the development of high-performance, earth-abundant electrocatalysts for sustainable, green H2 production.

Keywords: transition-metal dichalcogenides, density functional theory, hydrogen evolution reaction, molybdenum diselenide, electrocatalysis, electronic structure

1. INTRODUCTION

The increase in global temperatures motivates the search for sustainable energy alternatives. In this context, hydrogen energy has emerged as a potential candidate to facilitate the transition toward carbon-neutral systems. H2 energy can serve as a high-density, carbon-free fuel that emits water upon combustion or electrochemical conversion[1]. However, its sustainability depends entirely on its production method. Currently, 75% of the available H2 is produced via steam methane reforming (natural gas reacts with high-temperature steam to produce $H2_2$)[2]. This process releases significant amounts of CO_2 as a byproduct, and the resulting gas is classified as grey H[3]. To achieve green (i.e., CO_2 free) H2, research has shifted to electrochemical water splitting powered by renewable energy sources[4].

The cathodic half-cell reaction of the water-splitting process, where protons are reduced to molecular H2 through Volmer, Heyrovsky, and/or Tafel pathways[5], is known as hydrogen evolution reaction (HER). An efficient HER requires a catalyst that minimize the overpotential, thereby reducing the activation barrier. Although Pt and its alloys remain the benchmark owing to their optimal Gibbs free energies (close to zero) for H adsorption, their high cost and scarcity limit large-scale applications[6]. Consequently, earth-abundant alternatives, such as transition-metal dichalcogenides (TMDs), have emerged as leading alternatives.

TMDs, with general formula MX_2 (where M is a transition metal (TM) and X is a chalcogen), possess an anisotropic structure characterized by layers bonded together by weak van der Waals forces. This enables the exfoliation of TMDs into two-dimensional monolayers, yielding a high surface-to-volume ratio, which provides active sites ideal for catalytic applications[7]. Among the various TMDs, $MoSe_2$ has demonstrated significant potential owing to unique electronic structure; the highly covalent metal–selenide bond reduces the bandgap and enhances electrical conductivity compared to its metal-sulfide counterpart[8].

However, the catalytic activity of pristine $MoSe_2$ is fundamentally limited. Studies report that the basal planes are largely inert, with the HER activity being predominantly localized at the unsaturated Mo and Se edges[9]. Despite extensive efforts involving edge-site engineering and defect/doping strategies for

Published under an exclusive license by KFUPM

TMDs, the current understanding of how TM doping can selectively activate the basal plane through controlled electronic structure modulation remains limited. Particularly, the relationship among dopant-induced d-band tuning, orbital hybridization, and H adsorption energetics has not been fully elucidated. Regarding dopant-induced d-band tuning, Mo is replaced with various metal dopants, enabling alteration of the d-band electronic properties of the TM and the H adsorption free energy[9].

In this study, we utilize computational modeling to investigate the effects of 3d- and 4d-TM doping on the HER performance of $MoSe_2$ monolayers. We employ density functional theory (DFT) calculations to investigate a library of dopants (3d- and 4d-TM), quantifying their impact on the lattice stability, electronic structure, and catalytic activity. Beyond conventional single-descriptor screenings, this work pairs d-band center models with the electronic density of states and real-space electron localization functions topologies to map the trade-off between structural lattice stability and catalytic activity. By identifying dopants that tune the Gibbs free energy of the H adsorption toward zero, this study establishes a theoretical foundation for the design of high-performance and cost-effective HER electrocatalysts.

2. METHODOLOGY

The Vienna Ab initio Simulation Package (VASP) code, version 6.5.0.[10,11], was used to perform the spin-polarized DFT calculations. The projector augmented-wave method was used to describe the electron–ion interactions[12]. The exchange-correlation functional was treated within the generalized gradient approximation using the Perdew-Burke-Ernzerhof parameterization. A plane-wave basis set with a 500-eV kinetic energy cutoff was used for all calculations. The convergence criteria for the electronic and ionic relaxations were set to 10^{-5} eV and 0.01 eV/Å, respectively. Geometry optimization was conducted using a conjugated gradient algorithm with a $3 \times 3 \times 1$ Monkhorst-Pack k-point mesh for Brillouin zone sampling. To accommodate the van der Waals interactions, the DFT-D3 method with Becke–Johnson damping was used[13]. The density of states was calculated for the fully optimized structures using a denser $11 \times 11 \times 1$ k-point mesh. For surface calculation, we optimized the bulk $MoSe_2$ structure and constructed a 4×4 supercell with a 15-Å vacuum in the z-direction. We predicted the stabilities of the pristine and doped-$MoSe_2$ structures by calculating their formation energies using Eq. 1.

$$E_f = E_{doped} - 8E_{bulk} - \mu_{dopant} + \mu_{Mo} \quad (1)$$

Here, E_{doped} is the total energy of the doped supercell and $8E_{bulk}$ represents the energy of the bulk $MoSe_2$ unit cell comprising two layers, which are scaled to match the supercell stoichiometry. The μ_{dopant} and μ_{Mo} terms denote the chemical potentials of the TM dopant and host Mo atom, respectively, as derived from their respective bulk metallic phases.

We also calculated the Gibbs free energy of H adsorption on the Se site by doping two different Mo positions (the nearest neighbor of the adsorption site and the second-nearest site) using Eq. 2.

$$\Delta G_{H^*} = \Delta E_H + \Delta ZPE - T\Delta S \quad (2)$$

ΔG_{H^*} represents the Gibbs free energy change of hydrogen adsorption. ΔE_H is the electronic hydrogen adsorption energy derived directly from DFT total energy differences between the hydrogen-bound catalyst slab, the clean slab, and an isolated gas-phase H_2 molecule. $\Delta ZPE - T\Delta S$ denote the thermal correction term, consisting of the differences in zero-point energy and entropy, respectively, between the adsorbed intermediate state ($H*$) and gas-phase at absolute temperature. The d-band center was calculated using the VASP kit (version 1.5.1)[14].

3. RESULTS AND DISCUSSION

3.1. Structural Stability of Doped $MoSe_2$. The thermodynamic stabilities of the doped $MoSe_2$ monolayers were evaluated based on the total electronic energies of the fully converged geometries. Figure 1(inset) shows the predicted formation energies for 3d- and 4d-TM doping that replaced Mo on the $MoSe_2$ structure. As illustrated in Figure 1, negative formation energies were obtained for all doping elements, indicating the thermodynamic stability of the $MoSe_2$ doped structure. However, the formation energies of the early TMs, such as Ti, V, Zr, and Nb, were more negative than that of the pristine $MoSe_2$ (–1.11 eV), suggesting that incorporation of these elements is energetically more favorable than the use of pristine $MoSe_2$. This high compatibility implies minimal lattice strain, because the host framework effectively stabilizes these specific ions. Conversely, a clear increase in energy was observed as the d-orbital occupancy increased across the periodic table. That is, the lowest relative stability was observed for the late TMs (Cu, Ag, Zn, and Cd), with the energies shifting toward –0.81 eV. This trend was attributed to increased electron–electron repulsion and a growing population of antibonding states. These findings suggest that although all the investigated dopants yield stable configurations, the early TMs offer the highest structural integrity for the $MoSe_2$ framework.

3.2. Hydrogen Adsorption Energetics and Proximity Effects. To establish a baseline for the catalytic activity, the preferred H adsorption sites on the pristine $MoSe_2$ monolayer were first investigated. The adsorption energies were screened across three high-symmetry positions: the chalcogen radical site (Se), metal center (Mo), and interstitial hollow sites. The radical site was identified as the most stable configuration, having a ΔG_{H^*} of 1.40 eV. Higher energy barriers were observed at the metal center (1.68 eV) and interstitial hollow sites (2.42 eV).

Despite the relative stability of the chalcogen radical site, the strongly positive ΔG_{H^*} value highlights the inherent catalytic inertness of the pristine basal plane. To mitigate this energetic barrier, the impact of single-site metallic dopant proximity was analyzed by comparing two distinct structural arrangements: the first-nearest-neighbor (1NN) and second-nearest-neighbor (2NN) configurations relative to the Se active site (Figure 2). The findings for the 2NN configuration (Figure 2a) suggest that distant dopants provide insufficient electronic perturbation to significantly lower the energy barrier associated with the pristine structure. By contrast, a drastic reduction in ΔG_{H^*} was observed for the 1NN configuration (Figure 2 (b)). Notably, doping with Cd and Ag from the 4d-group tuned the adsorption energy to

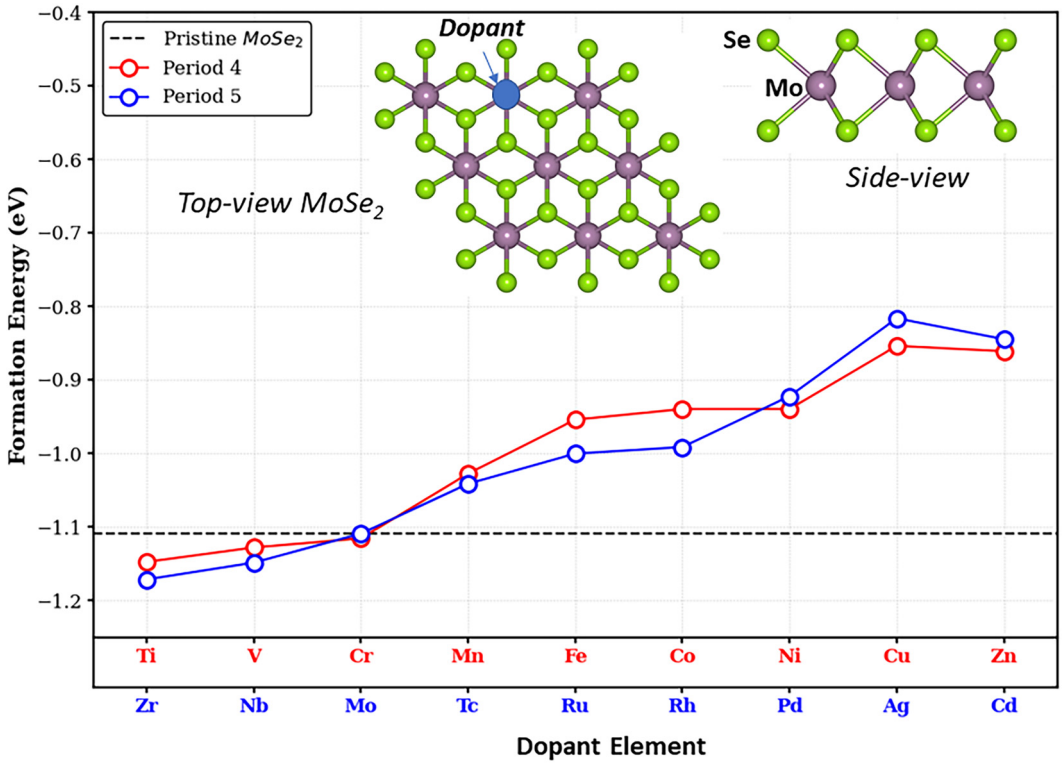

Figure 1. Doping stability (formation energy) relative to pristine $MoSe_2$. The dashed line represents the energy level of the pristine system

near-optimal values (–0.02 and –0.16 eV, respectively); these values signpost promising electrocatalysts for the HER.

This Gibbs free energy analysis provides important insights into the thermodynamic feasibility of elementary reaction steps and the adsorption behavior of key intermediates on the catalyst surface. However, further investigation into the electronic structure of the catalyst is required to understand the origins of these adsorption trends. Therefore, d-band center analysis was performed to establish the relationship between the surface electronic properties and the adsorption strengths of the reaction intermediates, as this relationship ultimately governs the catalytic activity and selectivity.

3.3. d-Band Center Scaling. In our analysis of the doped $MoSe_2$ systems, we found that knowledge of the electronic properties of the central active site alone is insufficient to enable full prediction of the catalytic performance; this finding mirrors observations made in recent coordination engineering studies [15]. As our active site was a non-metal (Se), its p- or d-band could not fully capture the traditional scaling relationship. A primary reason for this limitation is the significant structural deformation experienced by the active center upon adsorption, which alters the local electronic environment and reduces the reliability of the initial active-site descriptors.

In response to these limitations, we analyzed the electronic properties of the coordination atoms, as illustrated in Figure

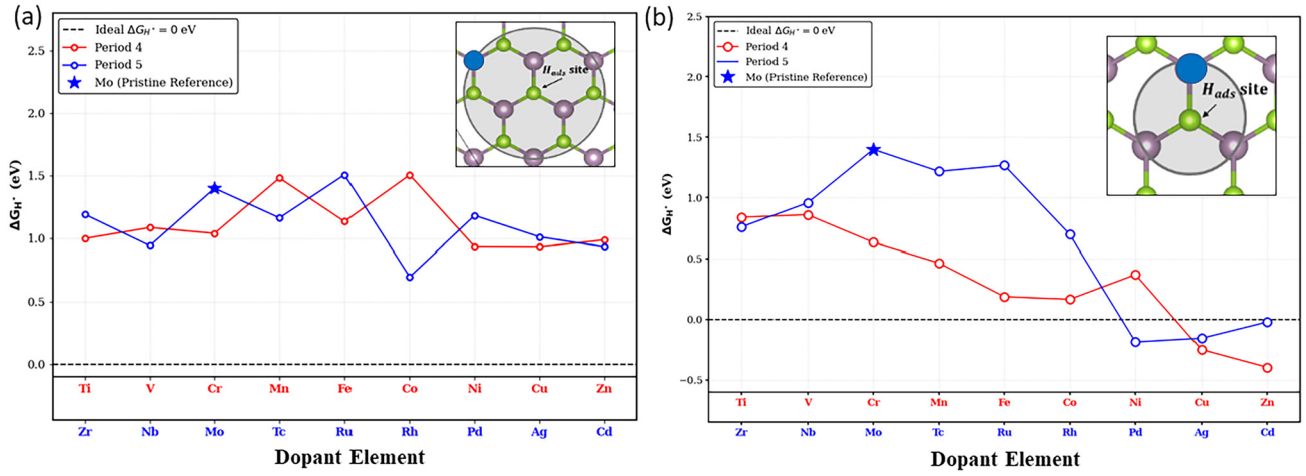

Figure 2. Comparison of H adsorption free energies (ΔG_{H^*}) on doped $MoSe_2$ monolayers at different adsorption sites: (a) 2nd and (b) 1st nearest neighbor (2NN and 1NN, respectively) configurations. The dashed horizontal line indicates the ideal thermo-neutral value ($\Delta G_{H^*} = 0$)

3(inset), in which the neighbors surrounding the active site are circled to indicate their roles as primary electronic modulators. Specifically, we examined the averaged d-bands of the metal atoms neighboring the Se site (the Mo atoms in the pristine system and the Mo and dopant combinations in the doped systems). This approach aligns with the principle that coordination atoms act as electron reservoirs and directly modulate the electron density at the active site through charge transfer. The relationships between the d-band center and H adsorption energy for each of the TM dopants are illustrated in Figure 3. A general linear trend is apparent. This suggests that the H binding strength weakens, shifting toward more positive ΔG_{H^*}, as the d-band center shifts closer to the Fermi level (becomes less negative). While most 3d- and 4d-TMs are clustered along the trendline in Figure 3, a few outliers, notably Zn, Cd, and Ru, are apparent. The existence of these outliers suggests that the local electronic environment and specific orbital interactions play a more nuanced role than a simple linear descriptor may imply. This variation underscores the importance of local atomic environment modulation in the fine-tuning of catalytic responses. Overall, the d-band center shows a near-linear correlation with the H adsorption energy; however, the deviations (e.g., Zn, Cd, and Ru) emphasize that the local electronic structure effects also play a critical role beyond that given by this simple descriptor.

3.4. Electron Localization Function (ELF) Analysis. To investigate the real-space distribution of the electrons and the nature of the chemical bonding, the ELF was calculated for three systems: pristine $MoSe_2$ (the least active), Cd-doped $MoSe_2$ (with optimal performance), and Zn-doped $MoSe_2$ (having the strongest adsorption). The calculation was performed for the systems both before and after H adsorption, as shown in Figure 4. Note that the ELF provides a dimensionless measure of electron localization, where values near 1.0 (red) and 0.0 (blue) indicate regions of high electron localization and electron-depleted zones, respectively.

The ELF map for the pristine $MoSe_2$ (Figure 4 (a)) reveals a periodic distribution of high-localization regions centered on the Mo and Se atoms. For the Cd- and Zn-doped systems (Figures 4 (b) and 4 (c)), however, the ELF maps exhibit slight electron delocalization from the Se atoms. This outcome indicates that the coordinated metals withdrew electrons from the Se, which was treated as an electron reservoir, as observed in the d-band center calculation. Significant differences in the bonding characteristics emerged with the introduction of H. The ELF profile obtained for the pristine $MoSe_2$ (Figure 4 (d)) revealed that the electrons remained largely localized around the adsorbed H atoms; this behavior indicates weak electronic interactions with the surface. Moreover, this outcome suggests limited charge sharing between the adsorbate and catalyst surface, which corresponds to relatively unfavorable adsorption behavior. By contrast, the ELF maps of the Cd-$MoSe_2$ and Zn-$MoSe_2$ systems (Figures 4 (e) and 4 (f), respectively) reveal a notable electron density overlap between the surface atoms and adsorbed H atom, thereby indicating stronger electronic interaction and enhanced bonding characteristics.

The electron sharing was more pronounced in the Zn-doped system, as is consistent with the shorter bond length and more favorable adsorption energy of this system. These results suggest that the Cd and Zn doping effectively modified the local electronic environment of the $MoSe_2$, thereby strengthening its interaction with H and improving its adsorption behavior.

3.5. Electronic DOS Analysis. To further investigate the electronic structure of the catalytic surface, we measured the total DOS (TDOS) for both the pristine and doped systems (Figure 5). The results provided direct evidence of the electronic modifications induced by the surface doping. Note that Ag- and Cd-doped systems were analyzed because of their superior adsorption performance compared to the pristine $MoSe_2$ electronic structure.

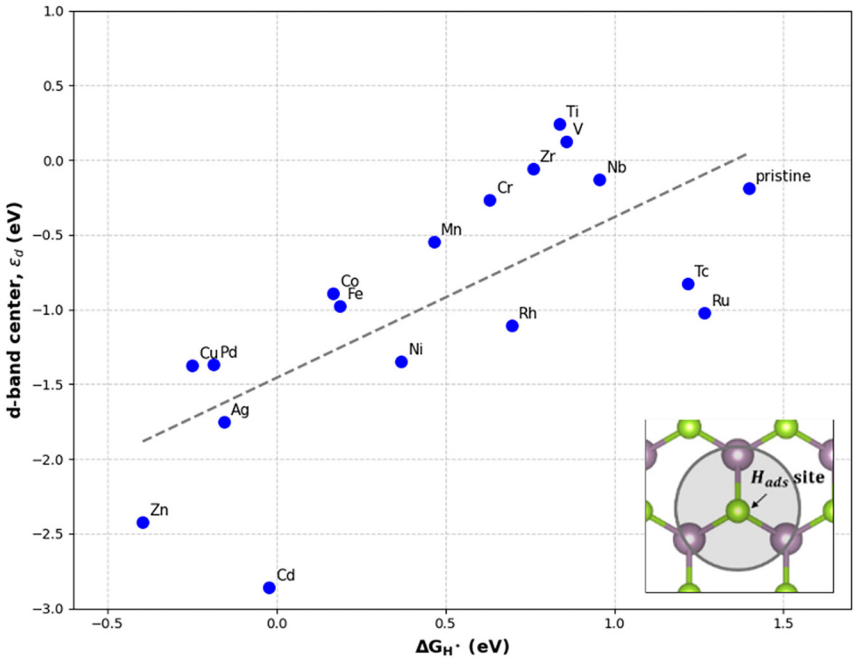

Figure 3. Correlation between d-band centers of coordinated TM dopants and Gibbs free energy of H adsorption (ΔG_{H^*}) on $MoSe_2$ monolayer

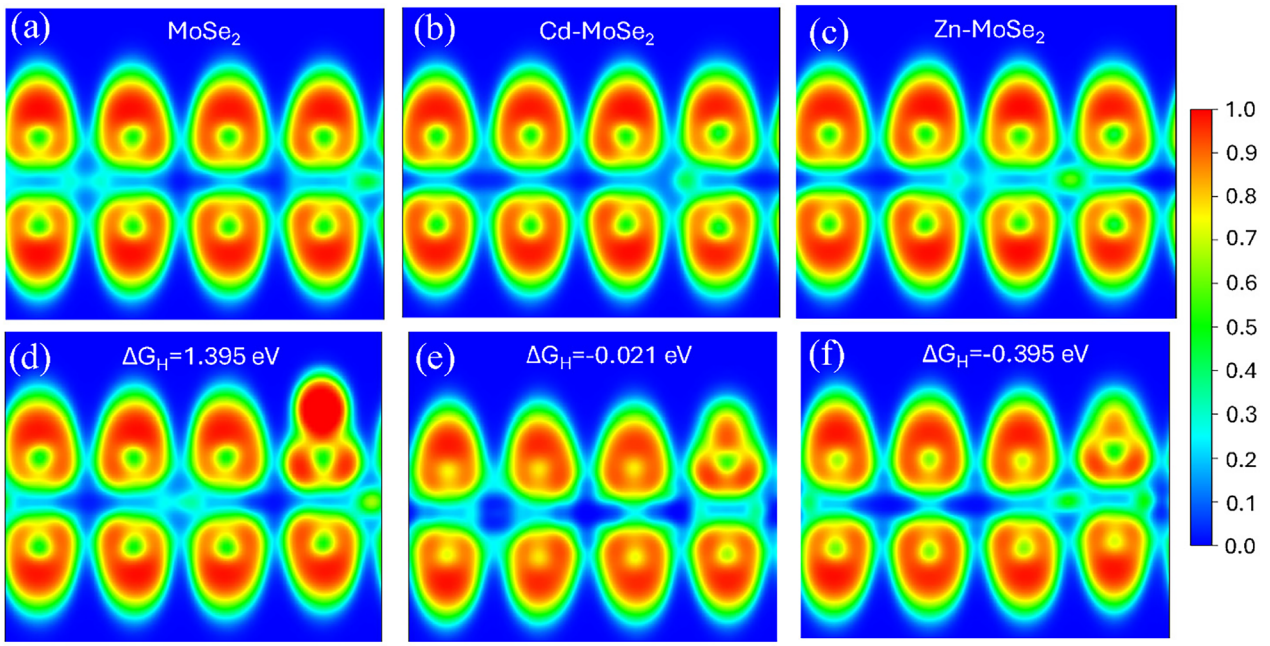

Figure 4. ELF maps of pristine and doped $MoSe_2$ monolayers. Figure 4. (a–c) ELF maps for (a) pristine, (b) Cd-doped, and (c) Zn-doped $MoSe_2$. (d–f) ELF maps illustrating H interaction on (d) pristine $MoSe_2$, (e) Cd-doped $MoSe_2$, and (f) Zn-doped $MoSe_2$. All slices correspond to the (1 0 0) plane at 7.8 Å from the origin

For the pristine $MoSe_2$ (Figure 5 (a)), a clear band gap around the Fermi level was obtained. This result is consistent with the semiconducting behavior of this material. By contrast, a finite DOS at the Fermi level was found for both the Ag- and Cd-doped $MoSe_2$ (Figures 5 (b) and 5 (c)), indicating dopant-induced metallization arising from the introduction of partially occupied d-derived states hybridized with the $MoSe_2$ lattice. Note that this enhanced electronic conductivity benefits the HER because it facilitates interfacial charge transfer.

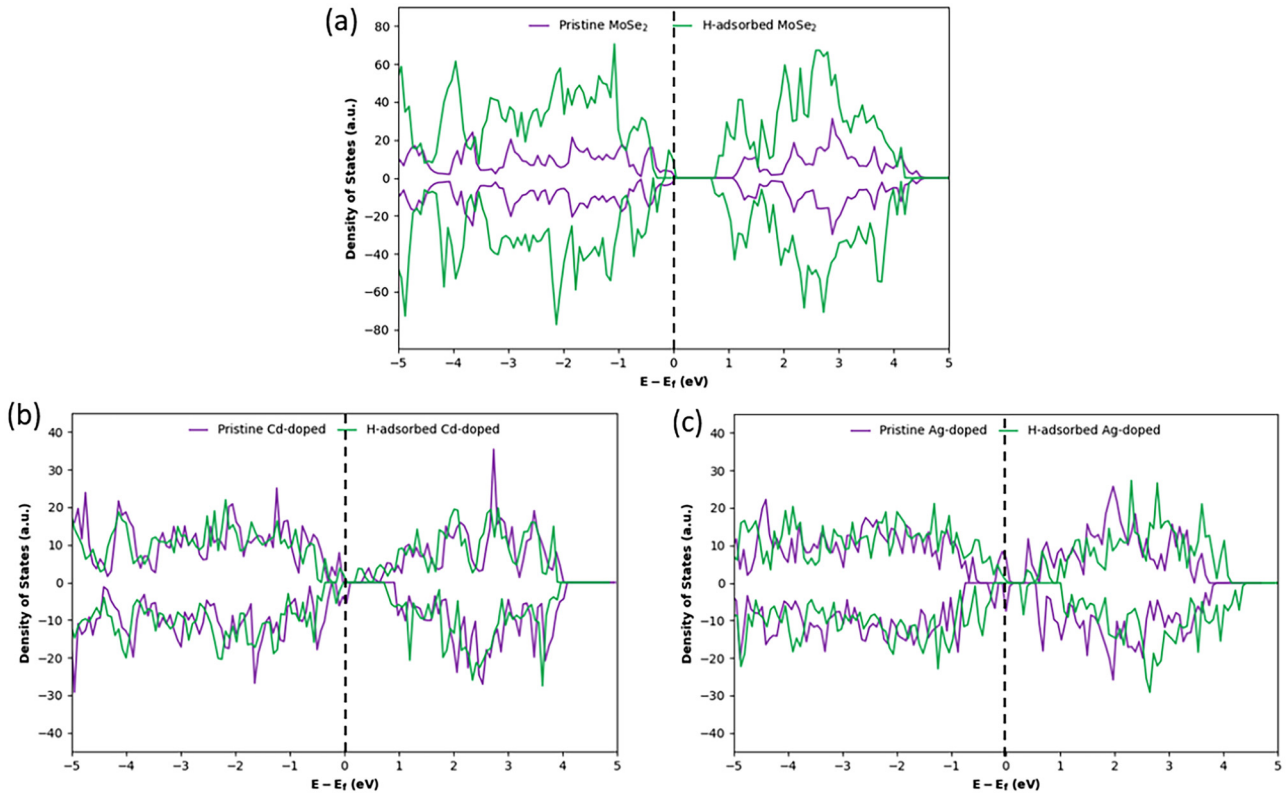

Figure 5. TDOS for $MoSe_2$ systems. The purple profiles represent the electronic states prior to H interaction, whereas the green profiles represent the post-adsorption states for (a) pristine, (b) Cd-doped, and (c) Ag-doped $MoSe_2$. The Fermi level (E_f) is set to 0 eV

Upon H adsorption, all systems exhibited significant DOS redistribution, which reflected the surface-adsorbate electronic coupling. For the pristine $MoSe_2$, H adsorption introduced mid-gap states, evidencing new covalent interactions with the surface atoms. However, the weaker redistribution and less favorable energetic separation of the bonding/antibonding states compared with those of the doped systems indicate weaker adsorption. In the Cd-$MoSe_2$ system, weaker peak broadening and reduced DOS perturbation near the Fermi level were obtained; this outcome suggests a less effective orbital overlap with H. That is, the antibonding states were closer to the Fermi level, which increased their partial occupation and reduced the net adsorption strength owing to the diminished bonding–antibonding splitting. In the Ag-$MoSe_2$ system, the broadening and downward shift of the states in the –2 to –5-eV range indicates strong Se p–H 1s hybridization, with stabilized bonding states forming well below the Fermi level. Concurrent to this downward shift, the antibonding states are pushed above the Fermi level; this minimizes their occupation and favors stronger adsorption.

Overall, the adsorption strength follows the energetic separation of the bonding and antibonding states: Ag doping maximizes this splitting and stabilizes the bonding states, whereas Cd doping reduces it, bringing the antibonding states closer to the Fermi level and weakening the H binding.

Ultimately, these electronic structure insights clarify why specific dopants shift the catalytic performance, providing a theoretical foundation that bridges our results with prior research. The baseline inertness of the pristine $MoSe_2$ basal plane ($\Delta G_{H^*} =$ 1.40 eV) supports existing literature asserting that TMD catalytic activity is heavily restricted to unsaturated edge sites [16]. The near-thermo-neutral values achieved by 1NN Cd (-0.02 eV) and Ag (-0.16 eV) doping validate experimental strategies focused on activating inert basal planes via localized transition metal substitution [17].

While this study provides a theoretical framework for activating the $MoSe_2$ plane, several methodological limitations must be noted. First, the calculations utilized flat, periodic 2D supercells under a vacuum, which omits real-world electrochemical factors such as solvent effects, pH variations, and the electrode-electrolyte interfacial electric field. Additionally, these models assumed perfect single-atom substitution in a flawless lattice framework. Real-world synthesized TMDs contain structural defects, such as selenium vacancies, grain boundaries, or edge disruptions that could interact with the dopants and alter the predicted electronic properties and catalytic pathways.

4. CONCLUSIONS

This study established a theoretical framework for activating the basal planes of $MoSe_2$ monolayers via TM doping so as to enhance the HER. DFT results revealed that early TMs doping (Ti, V, Zr, and Nb) provide the highest structural stability, whereas late TMs doping most effectively tune the catalytic activity. Particularly, Ag- and Cd-doping in the nearest-neighbor configuration reduce the H adsorption free energy (ΔG_{H^*}) from 1.40 eV (pristine $MoSe_2$) to near-thermo-neutral values of –0.16 and –0.02 eV, respectively. This improvement originates from dopant-induced metallization and a favorable d-band center shift, which together enhance the orbital hybridization between the dopant states and H 1s orbitals. ELF analysis further confirmed increased charge delocalization at the dopant–adsorbate interface. Overall, Ag- and Cd-doped $MoSe_2$ have emerged as promising and cost-effective alternatives to noble-metal catalysts for HER applications.

To build upon these theoretical insights, future research should focus on the experimental synthesis and electrochemical validation of these doped monolayers to verify their real-world overpotentials. Additionally, systematic investigations into the long-term stability and potential dopant dissolution mechanisms under continuous operating conditions are essential.

AFFILIATIONS AND AUTHOR DETAILS

Undergraduate Author

Zahra Ali Aljishi – *Department of Materials Science and Engineering, King Fahd University of Petroleum & Minerals, Dhahran 31261, Saudi Arabia*; 0009-0007-1044-4333
Email: s202251040@kfupm.edu.sa

Corresponding Author

Md Delowar Hossain – *Research Mentor, Assistant Professor, Department of Materials Science and Engineering, King Fahd University of Petroleum & Minerals, Dhahran 31261, Saudi Arabia*; 0000-0003-3440-8306
Email: mddelowar.hossain@kfupm.edu.sa

DECLARATION OF GENERATIVE AI AND AI-ASSISTED TECHNOLOGIES IN THE WRITING PROCESS

During the preparation of this work, the authors used ChatGPT to improve the language. After using this tool/service, the authors reviewed and edited the content as required. They take full responsibility for the resulting publication.

CONFLICT OF INTEREST

The authors declare no conflict of interest.

ACKNOWLEDGEMENTS

The authors acknowledge support provided by the Department of Materials Science and Engineering and the Interdisciplinary Research Center (IRC) of Hydrogen Technology and Carbon Management (HTCM) at the King Fahd University of Petroleum and Minerals (KFUPM). This research was funded by Project No. INHT2509. The authors also extend their appreciation to the IT staff and the staff of the High-Performance Computing (HPC) facilities at KFUPM.

REFERENCES

(1) Sharma, S., Agarwal, S. & Jain, A. Significance of hydrogen as economic and environmentally friendly fuel. *Energies* **14**, 7389 (2021).

(2) Karibe, H., Sair, S., Faik, A. & Ousaleh, H. A. Electrified steam methane reforming : a review of heating technologies, challenges, and prospects. *Int. J. Hydrogen Energy* **133**, 200–213 (2025).

(3) Pathak, P. K., Yadav, A. K. & Padmanaban, S. Transition toward emission-free energy systems by 2050: potential role of hydrogen. *Int. J. Hydrogen Energy* **48**, 9921–9927 (2022).

(4) Teli, A. M. *et al.* Development of electrochemical water splitting with highly active nanostructured NiFe layered double hydroxide catalysts: a comprehensive review. *Catalysts* **15**, 293 (2025).

(5) Lasia, A. Mechanism and kinetics of the hydrogen evolution reaction. *Int. J. Hydrogen Energy* **44**, 19484–19518 (2019).

(6) Cheng, Y., Wang, H., Qian, T. & Yan, C. Interfacial engineering of carbon-based materials for efficient electrocatalysis: recent advances and future. *EnergyChem* **4**, 100074 (2022).

(7) Saeloo, B. *et al.* Role of transition metal dichalcogenides as a catalyst support for decorating gold nanoparticles for enhanced hydrogen evolution reaction. *Inorg. Chem.* **63**, 18750–18762 (2024).

(8) Zhao, X. *et al.* $MoSe_2$ nanoplatelets with enriched active edge sites for superior sodium-ion storage and enhanced alkaline hydrogen evolution reaction. *Chem. Eng. J.* **382**, 123047 (2019).

(9) Mondal, A. & Vomiero, A. 2D transition metal dichalcogenides-based electrocatalysts for hydrogen evolution reaction. *Adv. Funct. Mater.* **32**, 101002 (2022).

(10) Kresse, G. & Hafner, J. *Ab initio* molecular-dynamics simulation of the liquid-metal–amorphous-semiconductor transition in germanium. *Phys. Rev. B* **49**, 14251 (1994).

(11) Kresse, G. & Furthmüller, J. Efficient iterative schemes for *ab initio* total-energy calculations using a plane-wave basis set. *Phys. Rev. B* **54**, 11169 (1996).

(12) Blöchl, P. E. Projector augmented-wave method. *Phys. Rev. B* **50**, 17953 (1994).

(13) Grimme, S. Semiempirical GGA-type density functional constructed with a long-range dispersion correction. *J. Comput. Chem.* **27**, 1787–1799 (2006).

(14) Wang, V., Xu, N., Liu, J. C., Tang, G. & Geng, W. T. VASPKIT: a user-friendly interface facilitating high-throughput computing and analysis using VASP code. *Comput. Phys. Commun.* **267**, 108033 (2021).

(15) Huang, H. *et al.* *p*-band center as the key descriptor: coordination engineering of single-atom catalysts for optimized oxygen electrocatalysis. *Ind. Eng. Chem. Res.* **64**, 23055–23066 (2025).

(16) Xie, J. *et al.* Defect-rich MoS_2 ultrathin nanosheets with additional active edge sites for enhanced electrocatalytic hydrogen evolution. *Adv. Mater.* **25**, 5807–5813 (2013).

(17) Tsai, C., Chan, K., Nørskov, J. K. & Abild-Pedersen, F. Rational design of MoS_2 catalysts: tuning the structure and activity via transition metal doping. *Catal. Sci. Technol.* **5**, 246–253 (2014).